Journal of Petroleum Exploration and Production Technology (2023) 13:917–927
https://doi.org/10.1007/s13202-022-01587-x

ORIGINAL PAPER - PRODUCTION ENGINEERING

Quantifying acid diversion efficiency through NMR tortuosity measurements

Mahmoud Elsayed[1] · Ahmed BinGhanim[1] · Murtada Saleh Aljawad[1] · Ammar El-Husseiny[1] · Ridha Al-Abdrabalnabi[1] · Mohamed Mahmoud[1]

Received: 14 July 2022 / Accepted: 8 November 2022 / Published online: 18 November 2022

Abstract

The diversion efficiency measures the acid capacity to change its flow direction to the lower permeability reservoir sections. A good acid diverter creates a tortuous (zigzagged) wormhole within the acidized core sample in a laboratory setup. Here, we studied two different acid diverters compared to the conventional hydrochloric acid (HCl) to investigate their efficiency in changing the wormhole direction inside the rock core. Nuclear magnetic resonance (NMR) can be used to measure the 3D tortuosity of a rock sample; hence, we propose it as a tool to measure acid diversion efficiency because it can be applied in the field and in the laboratory. Two acid systems were utilized: straight 15 wt.% HCl acid and gelled acid consisting of 15 wt.% HCl acid and polyacrylamide polymer (PAM). Four coreflooding experiments were conducted on 1.5 inch-diameter × 3 inch-length Indiana limestone samples, two with straight HCl acid and two with gelled HCl acid at different PAM concentrations. NMR was utilized to measure the T_2 distribution of the rock samples and diffusion tortuosity in two orthogonal directions. Also, X-ray computed tomography (CT) of the acidized samples was taken to visualize the wormholes. Results showed that the polymer-based acid-created zigzagged paths, and more acid volume was consumed to create the wormholes using CT. NMR diffusion tortuosity measurements showed that the tortuosity was reduced along the wormhole direction in all experiments. Nevertheless, the gelled acid treatments showed a significant reduction of the tortuosity orthogonal to the main wormhole path. The diversion efficiency of the 50 lbm/ 1000 gal PAM-gelled acid was 35% higher compared to the straight HCl acid. On the contrary, the 30 lbm/ 1000 gal PAM-gelled acid gave only 10% improvement in the diversion. The index could screen quantitatively which diverting acid is more efficient. We introduced a new diversion index based on the NMR diffusion measurements in this study to quantify the diversion capacity of an acid system in carbonate rock.

Keywords Matrix acidizing · NMR · Diffusion · Tortuosity · Diversion efficiency

Abbreviations

A	The Cross-Sectional Area of The Flow (cm^2)
a	Constant Depends on the Rock Properties
APGSTE	Alternating Pulsed Gradient Stimulated Echo
C	The Acid Diversion Efficiency Score
CMHPG	Carboxymethyl hydroxypropyl guar
CPMG	Carr-Purcell-Meiboom-Gill
CT	X-ray Computed Tomography
D	Free Diffusion Coefficients (m^2/s)
D_a	Damköhler Number
DPR	Normalized Maximum Differential Pressure
D_R	Acid Restricted Diffusion Coefficient(m^2/s)
G_x	Applied Magnetic Field Gradients in the X-direction (T/m)
G_y	Applied Magnetic Field Gradients in the Y-direction (T/m)
G	Magnetic Field Gradients (T/m)
g_0	Internal Magnetic Field Gradient (T/m)
g_a	The Applied Magnetic Field Gradient (T/m)
HCl	Hydrochloric Acid
HEC	Hydroxyethyl cellulose
HPG	Hydroxypropyl guar
I_d	The Diversion Index
k	The Rock Core Permeability (mD)
KCl	Potassium Chloride
KI	Permeability Improvement
L	Length Of The Core (cm)

✉ Mahmoud Elsayed
mahmoud.elsayed@kfupm.edu.sa

✉ Murtada Saleh Aljawad
mjawad@kfupm.edu.sa

[1] College of Petroleum Engineering and Geosciences, King Fahd University of Petroleum & Minerals, Dhahran 34464, Saudi Arabia

l	Pore Length (cm)
l_{wh}	Dimensionless Wormhole Length
MICP	Mercury Injection Capillary Pressure
NMR	Nuclear magnetic resonance
PAM	Polyacrylamide Polymer
PFG-NMR	Pulsed-Field Gradient Nuclear magnetic resonance
PSD	Pore Size Distribution
PVBT	The Pore Volume Injected Until The Breakthrough.
Q	The Injection Flow Rate (cm^3/min)
q	Injection Flow Rate (cm^3/min)
RF	Radio Frequency
S/S_0	NMR Signal Attenuation
S/V	The Surface-to-Volume Ratio.
SNR	Signal-To-Noise Ratio
T_2	The Transverse Relaxation Time (ms).
$T_{2,bulk}$	The Bulk Fluid Transverse Relaxation Time(ms).
$T_{2,surface}$	The Rock Surface Transverse Relaxation Time(ms).
$T_{2,diffusion}$	The Fluid Diffusion Transverse Relaxation Time(ms).
t_e	Echo Time
VES	Viscoelastic Surfactant

Greek Letters

δ	Time Between Two Magnetic Field Gradients(ms).
Δ	Diffusion Time(ms).
γ	Gyromagnetic Ratio (rads/s.T)
δ_1 and δ_2	The Pre- and Post-Pulse Time(ms).
ΔP	The Pressure Drop (psi).
μ	Fluid's Viscosity (cp)
ρ_2	The Surface Relaxivity (μm/ms)
$\Phi_{pre\text{-}acid}$	Porosity of the Rock Core before Acid Treatment
$\Phi_{post\text{-}acid}$	Porosity of the Rock Core after Acid Treatment
τ_D	Diffusion Tortuosity
$\tau_{D,x}$	Diffusion Tortuosity In The X-Direction
τ_D,y	Diffusion Tortuosity In The Y-Direction

Introduction

Matrix acidizing is a well stimulation method that is applied to improve rock permeability and/or remove formation damage. The acid creates high permeability paths (i.e., wormholes) in carbonate rocks that bypass the damaged zone. In heterogeneous formations, acid overstimulates the high permeable sections of the reservoir, leaving the other tight sections unstimulated. Hence, various types of diverters are applied to direct the acid toward the tight rock sections, creating uniform stimulation (Aljawad et al., 2019). The reaction and the transport of acid inside the formation are governed by different process such as the reversible surface reaction, fluid transport to the rock, and the product transport away from the rock surface (Fredd and Fogler 1998). By taking into account all these processes, the rock dissolution is observed to depend on Damköhler number (D_a) that needs to be optimized in order to reach breakthrough with the minimum number of injected pore volume (Fredd and Fogler 1999). The Damköhler number defines the ratio of the total rate of dissolution occurs by acid to the rate of acid convection, and it governed by the following equation:

$$D_a = a\left(\frac{D_R^{\frac{2}{3}} l}{Q}\right) \tag{1}$$

where a is constant depends on the rock properties, D_R is the acid restricted diffusion coefficient (m^2/s), l is the pore length (m), Q is the injection flow rate (m^3/s). The Q is controllable factor while D_R depends on the acid properties. Hence, an accurate determination of diffusion coefficient is extremely important to be obtained using an independent measurement such as rotating disk or NMR diffusion experiments (Hoefner and Fogler 1989).

Different diverter types have been applied in acid stimulation: mechanical, viscous fluids, and solid particles. Mechanical diverters depend on tools to isolate a reservoir section, such as packers and ball sealers. Coil tubing is considered a mechanical diverter used to inject acid in the desired zone directly. On the other hand, solid diverters are small particles that are carried by fluids to accumulate and temporarily plug the high permeable zones, forcing the acid toward the low permeability sections. Fibers, wax beads, benzoic acid flakes, and rock salts are common solid diverters that are implemented in the field.

On the other hand, fluid diverters are the primary stimulating fluids that could be acid-based. The fluid viscosity increases during the acid reaction, which creates the diversion effect in-situ. These fluids could be based on the crosslinked gel, emulsifiers, viscoelastic surfactant (VES), foamers, etc. (Altunina et al. 2019; Zhang et al. 2021; Adewunmi et al. 2022). Polymer hydration creates gelled fluid; guar derivatives are the most common in the oil and gas industry. Carboxymethyl hydroxypropyl guar (CMHPG), hydroxypropyl guar (HPG), hydroxyethyl cellulose (HEC), and polyacrylamide polymer (PAM) are usually used due to their fast hydration and low cost. A metal crosslinker is added to increase the gel viscosity and achieve better diversion. Borate is added as a crosslinker at high pH, while zirconium is usually used in a low pH environment (Barati and Liang 2014). One of the latest stimulation technologies

is the double action emulsified acid which showed a great potential both in laboratories and field-scale trails. This technique gained its impotence because of its delayed reaction allowing a deeper stimulation job and less corrosion to the downhole tools. A novel emulsified acid was also invented that combine the previous advantages in addition to its capability to dissolve paraffin deposits that could clog the created wormhole (Martyushev and Vinogradov 2021; Derendyaev et al. 2022). Not only the fluid but also the carbonate rock mineralogy (limestone or dolomite) could play a major role in acid dissolution process. Recent study revealed that increasing the holding time of the acid and dolomitic rock interaction does not always guarantee an efficient acid job (Martyushev and Novikov 2020; Martyushev et al. 2022). The acid-rock reaction products could cause wormhole clogging that could decrease the rock permeability with increasing the holding time.

NMR is a powerful and non-destructive tool that has been widely used both in laboratory and field-scale as a wireline logging tool (Elsayed et al. 2022). Reliable measurements of fundamental petrophysical properties such as porosity, pore size distribution, permeability, and wettability can be obtained using NMR T_2 relaxation time measurement (Timur 1969; Kenyon 1997; Straley et al. 1997; Al-Garadi et al. 2022). T_2 relaxation time reflects the pore size distribution of single-fluid saturated rocks; hence, pore connectivity could be evaluated (Vogt et al. 2014). Accurate determination of pore size distribution (PSD) of the carbonate rocks using the mercury injection capillary pressure (MICP) or NMR could be of great importance for a successful acid job (Shafiq et al. 2018). Three different Indiana limestone rock core plugs with different PSD (micropore-dominated, micropore and macropore, and macropore dominated) were characterized using MICP, then they were acidized (Yoo et al. 2019). The authors concluded that micropore-dominated rocks undergo slower reaction rate and lower diffusion although samples all samples have the same mineralogy. Hence, ignoring the PSD characterization could lead to under–or overestimation of optimum reaction and diffusion coefficient. Several attempts were performed using NMR before and after the acidizing to evaluate the changes in the porosity and pore sizes after creating the wormhole (Al-Duailej et al. 2013; Mahmoud et al. 2016). NMR T_2 relaxation time measurement captured the interconnectivity between the pore sizes qualitatively, which was indicated by the occurrence of larger T_2 components (wormhole) coupled with the ones before acidizing. However, this technique could not capture the degree of sinuosity along the flow direction (i.e., tortuosity) and the branches of the wormhole created in the perpendicular direction.

Pulsed-field gradient (PFG) NMR is considered as one of the most robust and accurate techniques to measure the free and restricted diffusion coefficients (D, D_R) of fluids inside porous media. PFG-NMR was firstly demonstrated by Stejskal and Tanner, based on the application of two magnetic field gradients (g) in opposite directions during (δ) separated by diffusion time (Δ) (Stejskal and Tanner 1965). Then, the diffusion of the NMR-bearing sample can be detected during Δ, which will result in NMR signal attenuation (S/S_0) that is calculated using the following equation.

$$\frac{S}{S_0} = \exp\left(-D(\gamma g\delta)^2\left(\Delta - \frac{\delta}{3}\right)\right) \tag{2}$$

where γ is the gyromagnetic ratio of the nucleus under investigation (2.68×10^8 rads/s.T, for ^{1}H). The deployment PFG-NMR technique showed a great potential to characterize pore structure and pore size distribution of several types of porous media for different applications based on the diffusion coefficient (Callaghan et al. 1991; Sen 2004; Kashif et al. 2019). The ratio between the free-bulk diffusion coefficient to the restricted-fluid (inside porous medium) diffusion coefficient is well-known as the diffusion tortuosity (τ_D) as per the following equation (Clennell 1997; Yang et al. 2019):

$$\tau_D = \frac{D}{D_R} \tag{3}$$

For ideal packing of similar grain size material, $\tau_D \approx 1.4$ (Blackwell 1962); however, it becomes higher for rock core plugs due to the pore structure's complexity. Outcrop Berea sandstone showed a range ($2.4 < \tau_D < 3.5$); other sandstone such as Fontainebleau and Navajo showed values between 3.1and 4.9. On the other hand, carbonate rock plugs (i.e., Indiana Limestone) showed higher tortuosity values ($7.8 < \tau_D < 12.2$) based on permeability (Hurlimann et al. 1994). The diffusion tortuosity can be measured in different directions depending on the applied magnetic field gradient. Thus, diffusion tortuosity anisotropy can be obtained by measuring the diffusion tortuosity in perpendicular directions independently. Diffusion tortuosity anisotropy is involved in a wide range of applications including energy storage (Long et al. 2004; Liu and Liu 2012), catalysis (Kolitcheff et al. 2018), bioengineering (Dvir et al. 2011), and oil & gas industry (Backeberg et al. 2017; Elsayed et al. 2021a). PFG-NMR was successfully implemented to locate the preferential direction of fracture by measuring the diffusion tortuosity along three directions (x, y, and z) of sandstone and carbonate rock core plugs (Elsayed et al. 2021c).

This study evaluates the diversion efficiency of acid in an acidized core sample by measuring the diffusion tortuosity along and perpendicular to the flow directions. The index of diversion was introduced in this work which indicates the diversion capacity of an acid system. To the best of the authors' knowledge, this is the first study showing

how PFG-NMR measurements could evaluate the diversion efficiency in matrix acidizing.

Acid diversion index and its evaluation techniques

The calculation of wormholes tortuosity to evaluate the efficiency of acid diversion capacity and performance has obtained a great attention recently, defined a new terminology called the wormhole length ratio that is defined as the length of longest wormhole created by VES acid to that of regular acid (Liu and Liu 2016). This would help comparing the acidizing effect between VES acid and conventional acid. A recent study came up with a comprehensive index of diversion performance that takes into account the following factors: stimulation performance (l_{wh} = dimensionless wormhole length), plugging effect (KI = permeability improvement), and maximum differential pressure (DPR = normalized maximum differential pressure) (Cao et al. 2021). This index can be calculated using the following equation:

$$C = DPRx4 + KIx3 + l_{wh}x3 \quad (4)$$

where C is the acid diversion efficiency score (Poor if $0 < S < 3$; medium $4 < S < 6$; better if $7 < S < 10$).

There are multiple methods to evaluate the diversion capacity of an acid system. In field operations, diversion capacity is evaluated by monitoring the increase of surface pressure as the diverter interacts with the formation. The diversion could be evaluated in laboratory setup through the dual-coreflooding system or CT scan imaging. However, performing dual-coreflooding experiments is expensive and subject to experimental failures. On the other hand, CT scan images only provide qualitative analysis of the diversion capacity. Numerical simulators can be used to evaluate diversion, but they require detailed and accurate rheology and reaction data, which are seldom available. Hence, we proposed to use PFG-NMR measurements to quantify the diversion capacity of an acid system. Table 1 summarizes the available techniques in the literature to measure the diversion capacity of an acid.

Methodology

Materials

Two different acid types were used in coreflooding experiments, as shown in Table 2. The first fluid system consists of 15 wt.% HCl acid without additives (i.e., straight HCl acid). The second fluid system is made of 15 wt.% HCl with different percentages of polyacrylamide polymer (PAM) with

Table 2 Types of acidic fluids used in core flooding experiments along with the rock sample

Experiment set	Rock sample	Base fluid	Polymer
A	Ind-1	15% HCl	0%
	Ind-2	15% HCl	30 lbm/1000 gal PAM
B	Ind-11	15% HCl	0
	Ind-22	15% HCl	50 lbm/1000 gal PAM

Table 1 Summary of the techniques used to measure acid diversion

Evaluation Technique	Indicator	Advantages	Disadvantages	References
Dual-Coreflooding	-Maximum pressure drop ratio -Permeability ratio	-Real-time data -Direct measurements	- Inability to visualize the wormhole from inside the core plug	(Zerhboub et al. 1994; Al-Ghamdi et al. 2014; Zakaria and Nasr-El-Din 2016; Du et al. 2019)
CT imaging	Wormhole shape	Visual representation of the zigzagged pathway	-Resolution (wormhole below resolution capability could not be captured) -Indirect measurements (requires segmentation and filtering that could be subjective to human error)	(Hoefner and Fogler 1989; Liu and Liu 2016; Cao et al. 2021; Novikov et al. 2022)
Numerical Modeling	Wormhole shape	Visual representation of the zigzagged pathway	Requires accurate input of fluid rheology and kinetics Approximation of the true solution	(Cheng et al. 2002; Panga et al. 2005; Aljawad 2020; Ba Alawi et al. 2020; Wu et al. 2022)
Analytical Methods	Effective tortuosity	Accurate solution	Only applicable for simple acidizing process Difficult and not always possible	(Fredd and Fogler 1998; Strongylis and Papamichos 2021; Alarji et al. 2022)

Table 3 Rock samples (Indiana limestone) properties

Sample ID	L (cm)	D (cm)	Permeability (mD)	Porosity (%)
Ind-1	7.259	3.793	3.96	15.7
Ind-2	7.473	3.802	1.66	15.8
Ind-11	7.159	3.795	0.73	10.2
Ind-22	7.396	3.798	0.80	12.2

the formula (-$CH_2CHCONH_2$-). Samples Ind-1 and Ind-11 were treated with HCl acid, whereas samples Ind-2 and Ind-22 were acidized with gelled acid (i.e., polymer-based acid). Standard core plugs (1.5-inch × 3-inch) of Indiana limestone (Ind) were utilized. The rock samples in the first set of experiments (A) have high permeability and porosity. The properties of the rock samples are summarized in Table 3.

Experiments

NMR: The NMR measurements, including T_2 and diffusion, were performed at room temperature using Oxford instruments MARAN DRX 12 MHz NMR Rock core analyzer. The system is featured with a three-dimensional magnetic field gradient with a maximum magnitude of 0.3 T/m and a 53-mm inner diameter radio frequency (RF) coil.

Carr-Purcell-Meiboom-Gill (CPMG) pulse sequence were performed to acquire the T_2 relaxation time distribution (Carr and Purcell 1954; Meiboom and Gill 1958). The T_2 relaxation time distribution of porous medium is correlated to the confined pore size according to the Brownstein–Tarr equation and can be modeled as follows:

$$\frac{1}{T_2}=\frac{1}{T_{2,bulk}}+\frac{1}{T_{2,surface}}+\frac{1}{T_{2,diffusion}}=\frac{1}{T_{2,bulk}}+\rho_2\frac{S}{V}+\frac{D}{12}(\gamma g t_e)^2 \quad (5)$$

where $T_{2,bulk}$ is the transverse relaxation time of the bulk-free fluid (ms), ρ_2 is the surface relaxivity (μm/ms), S/V is the surface-to-volume ratio ($\mu m^2/\mu m^3$), t_e is the echo time between the 180° RF refocusing pulses during the CPMG train (ms). By choosing the $t_e = 0.1$ ms, the effect of the internal gradient is minimized (Connolly et al. 2019; Elsayed et al. 2021b), and T_2 becomes a direct indication of the pore sizes. Furthermore, the signal-to-noise ratio (SNR) was kept at 100, the number of echoes was 5,000, and the recycle delay was 10,000.

For the PFG-NMR measurements, the "13-interval" alternating pulsed gradient stimulated echo (APGSTE) NMR pulse sequence was used for the diffusion measurements to reduce the effect of the internal gradient; it was modeled as the following equation (Cotts et al. 1989):

$$\frac{S}{S_0}=\exp\left\{-D\gamma^2\left[\delta^2\left(4\Delta+6\lambda-\frac{2\delta}{3}\right)g_a^2+2\lambda\delta(\delta_1-\delta_2)g_a g_0+\frac{4}{3}\lambda^3 g_0^2\right]\right\} \quad (6)$$

where λ is the duration between the first two RF pulses (ms), g_a and g_0 are the applied, and internal magnetic field gradient (T/m), respectively, δ_1 and δ_2 are the pre- , and post-pulse time (ms), respectively. The previous equation can be simplified by choosing δ_1 and δ_2, and sets $\Delta >> \lambda$; this will eliminate the second and the third terms, respectively. The equation becomes:

$$\frac{S}{S_0}=\exp\left\{-D\gamma^2\left[\delta^2\left(4\Delta+6\lambda-\frac{2\delta}{3}\right)g_a^2\right]\right\} \quad (7)$$

Table 4 lists a summary of the experimental parameters chosen for the NMR-PFG measurements. Note that the gradient strength was adjusted to ensure total signal attenuation approaches the noise level.

It is worth mentioning that all NMR measurements were performed with brine (3 wt% KCl) saturated rock core plugs. Heat shrink was utilized around the rock core plugs and at the inlet to ensure no loss for saturation. In order to obtain the diffusion tortuosity (τ_D), we follow this step-by-step procedure:

1- Measure the free-bulk fluid diffusion coefficient (D); in our case, the fluid is brine (3wt% KCl). The brine was filled in Teflon container that is NMR-silent material to ensure the detectable signal is only received from the brine. The diffusion coefficient of the brine showed a value of (2.37×10^{-9} m^2/s). This value does not change with increasing the diffusion time because the fluid is not confined to porous media.
2- Measure the restricted diffusion coefficient (D_R) at different diffusion times (Δ) until no change in the value of D_R is observed as illustrated in Fig. 1. This is done to guarantee that the molecules traveled through all the geometric restrictions of the pore space. This step should be performed by applying the magnetic field gradient in one direction ($\tau_{D,x}$) and then repeated in the orthogonal direction ($\tau_{D,y}$).

Table 4 NMR-PFG experimental parameters

Parameters	Value
Small delta, δ	1.5 ms
Duration between the first two RF pulses, λ	3 ms
Diffusion time, Δ	100–1200 ms (every 100 ms)
Number of scans, (NS)	16
Recycle delay, (RD)	10,000 ms
Gradient strength range (T/m)	0 < Gx < 0.25, 0 < Gy < 0.25

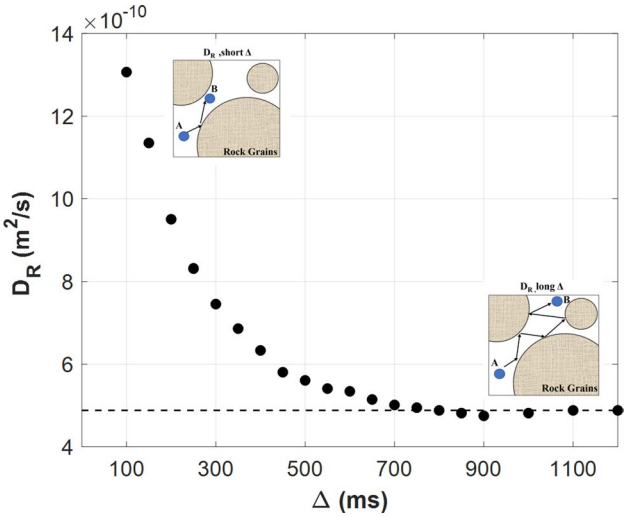

Fig. 1 D_R /D_0 as function of diffusion time for the core plugs used in this study. Note that these data were acquired for the measurements performed by applying the magnetic field gradient in the Y-direction

3- A plot of D/D_R as a function of different diffusion times is used to obtain the τ_D value; that is the value where no change in the D/D_R is observed as the diffusion time increases. Some scholars define the diffusion tortuosity using PFG-NMR as Eq. 2 (Latour et al. 1993; Frosch et al. 2000):

Coreflooding: In general, Coreflooding experiments are designed to test rock samples' interaction with fluids while controlling the pressure, temperature, and flow rates. From the flow rate and pressure drop data, the permeability is measured using Darcy's law:

$$k = 245\frac{q\mu L}{A\Delta p} \tag{8}$$

where k is the rock core permeability (mD), q is the injection flow rate (cm^3/min), A is the cross-sectional area of the flow (cm^2), μ is fluid's viscosity (cp), L is given distance (length of the core) for the pressure drop (cm), and ΔP is the pressure drop (psi).

A confining pressure of 1,500 psi and backpressure of 1,000 psi was maintained during coreflooding experiments. All acidizing experiments were performed at room temperature while the acid injection rate was 1 cm^3/min. For the duration of the experiment, the pressure is monitored until a zero-pressure drop is observed. The pore volume injected until the wormhole breakthrough the sample was recorded (PVBT).

Procedure

The methodology used to prove the concept is shown in Fig. 2. First, the porosity and permeability of four Indiana limestone rock samples were measured. NMR is then used to measure the rock porosity and pore size distribution (PSD).

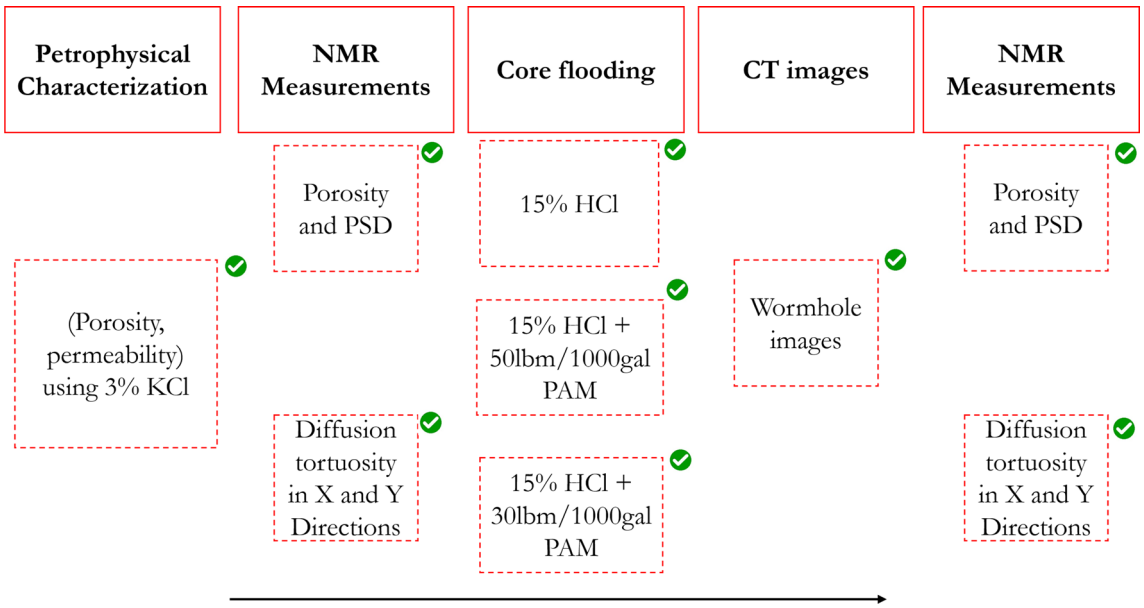

Fig. 2 Schematic representation of the restriction caused by the pore structure that leads to reduction in diffusion coefficient. It is worth mentioning that the Δ values used in this schematic diagram do not correspond to the measurements done in this study, they are only used for better visualization to the concept of PFG-NMR at short- and long-time regime

It was also used to measure diffusion tortuosity in two orthogonal directions. These are the X-direction (orthogonal to wormhole propagation direction) and Y-direction (parallel to wormhole propagation direction). Then coreflooding was conducted by injecting two different HCl acid systems into the core samples until wormhole breakthrough. As shown in Fig. 2, these are straight HCl and polymer-based HCl at different polymer concentrations. CT scan is then used to image the treated samples to visualize the wormhole created. Finally, similar NMR measurements were conducted after the treatment to evaluate the wormhole.

Results and discussion

Four rock samples were characterized as illustrated in Table 3. It can be observed that set (A) has the same dimensions (1.5-inch × 3-inch) and similar porosity but slightly different permeability, and the same is valid for the set (B) but with lower permeability and porosity. Figure 3 shows the recorded pressure drop during the acid injection. The acid is injected until the pressure drop reaches zero, indicating a wormhole breakthrough. Notice that PVBT is higher for the polymer-based acid (i.e., gelled acid) than straight acid, considering both sets of experiments. Also, the higher the polymer concentration, the higher the required treatment volume.

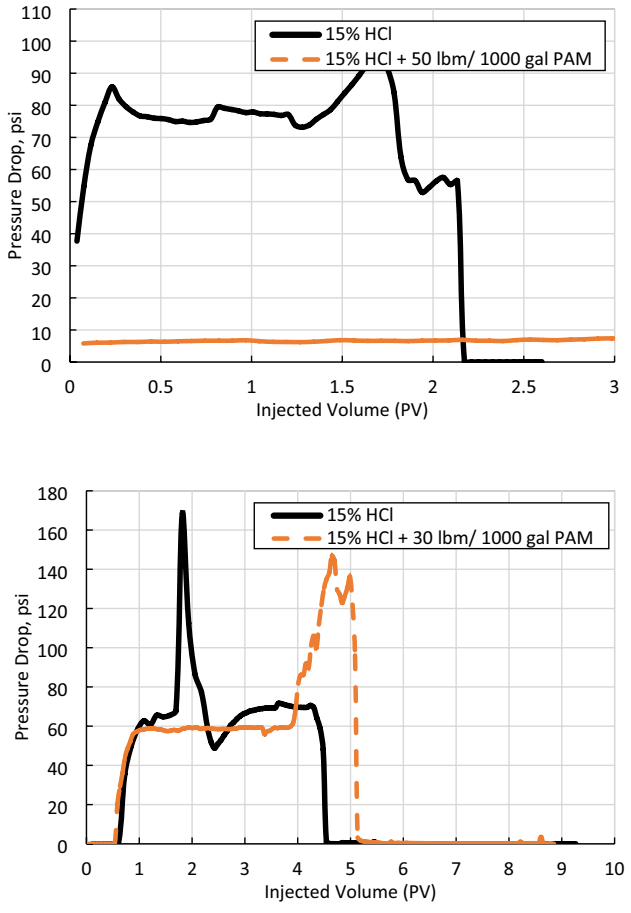

Fig. 3 Experimental methodology to evaluate acid divergence through NMR tortuosity measurement

Figure 4 shows the CT scan images of wormholed samples with and without diversion (i.e., PAM). Figure 4a shows that the straight HCl acid created a straight wormhole compared to the zigzagged wormhole created by the gelled acid. Larger wormholes were created in the inlet of the sample treated with the polymer-based acid. A similar conclusion can be observed in Fig. 4b, although the diversion of gelled acid was not as obvious visually. Because gelled acid resists traveling in the direction of flow, it has flow components in the direction perpendicular to the wormhole propagation, which enhances acid diversion. Table 5 shows the porosity values of the samples before and after treatment, indicating that the gelled acid results in a higher increase in porosity. This is attributed to the larger volume of acid needed for the wormhole to penetrate the sample.

Figure 5 shows the T_2 relaxation time distributions for the samples used in this study. It is worth mentioning that the T_2 distributions before acidizing (red-dotted curves) were almost identical for both samples; hence, one T_2 distribution was plotted for each sister plug. Furthermore, the T_2 distributions of the samples before acidizing have a single dominant peak which indicates a single pore system. After the injecting of acid, the samples were also analyzed. Figure 5a showed changes in the pore size distribution indicated by the increase in the distribution's probability density (NMR porosity), which agree with the helium porosity measurements tabulated in Table 5. In addition, larger T_2 components (~5,000 ms) appeared, implying more freedom to the hydrogen spins caused by the pore size enlargement. It can be noticed that there is a slight separation between different pore systems due to the wormhole. Figure 5b shows similar behavior except for the clear separation between the pore systems. The important point is that both T_2 distributions after acidizing for each sister plug showed the same T_2 components (x-axis), although there were treated using different acids. Therefore, T_2 relaxation time measurements could distinguish the diversion efficiency only from the increment in the porosity (y-axis), assuming that higher diversion efficiency results in high porosity. T_2 distributions neither provide information about the pathway of the wormhole nor the direction.

Figure 6 shows the diffusion tortuosity measured in the y-direction of the samples. Notice that the diffusion coefficient drops initially and reaches an asymptotic value at longer diffusion times. At these long diffusion times, molecules diffuse through the large pore spaces, and hence *DR* level does not change with time. The inverse

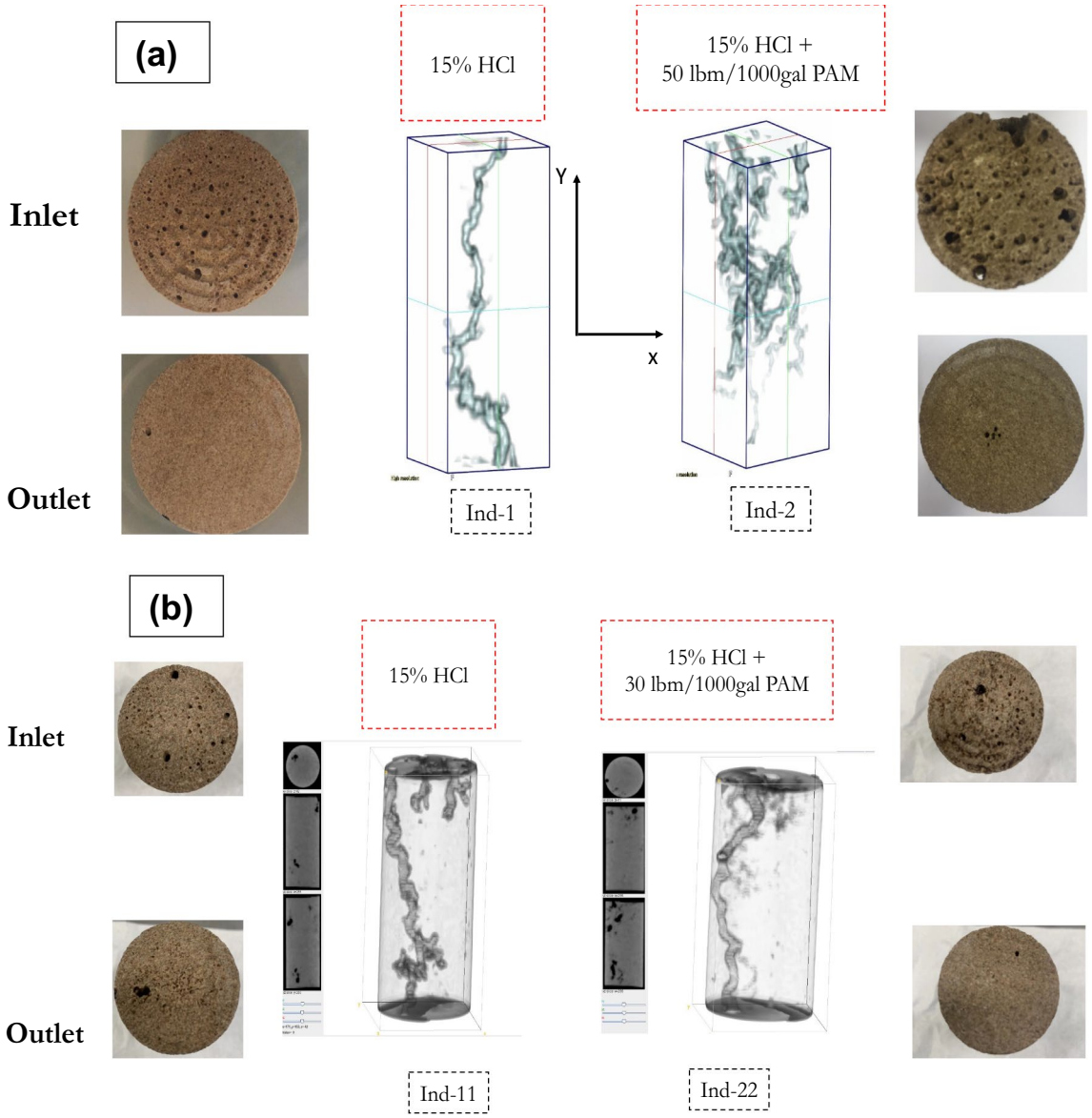

Fig. 4 **a** Pressure drop during acid Coreflooding in set (A) experiments, **b** Pressure drop during acid Coreflooding in set (B) experiments

Table 5 Petrophysical characterization of the rock samples

Sample ID	Base fluid	L (cm)	D (cm)	k (mD)	$\Phi_{pre\text{-}acid}$ (%)	$\Phi_{post\text{-}acid}$ (%)	% Increase in ϕ
Ind-1	15% HCl	7.259	3.793	3.96	15.7	16.3	3.8
Ind-2	15% HCl + 50 lbm/1000 gal PAM	7.473	3.802	1.66	15.8	19.18	21.3
Ind-11	15% HCl	7.159	3.795	0.73	10.2	10.31	1.07
Ind-22	15% HCl + 30 lbm/1000 gal PAM	7.396	3.798	0.80	12.2	13.81	13.2

of the asymptotic value represents the diffusion tortuosity. Table 6 shows the calculated values of the diffusion tortuosity before and after acidizing. In general, large open spaces within the rock tend to reduce the rock tortuosity, and hence the wormholes do. If tortuosity reduction in both X- and Y-directions is similar, acid diversion is thought to be effective. That usually happens when a zigzagged wormhole is created, as in the PAM treatment of the Ind-2 and Ind-22 samples. On the other hand, the straight wormholes created by straight and HCl acids

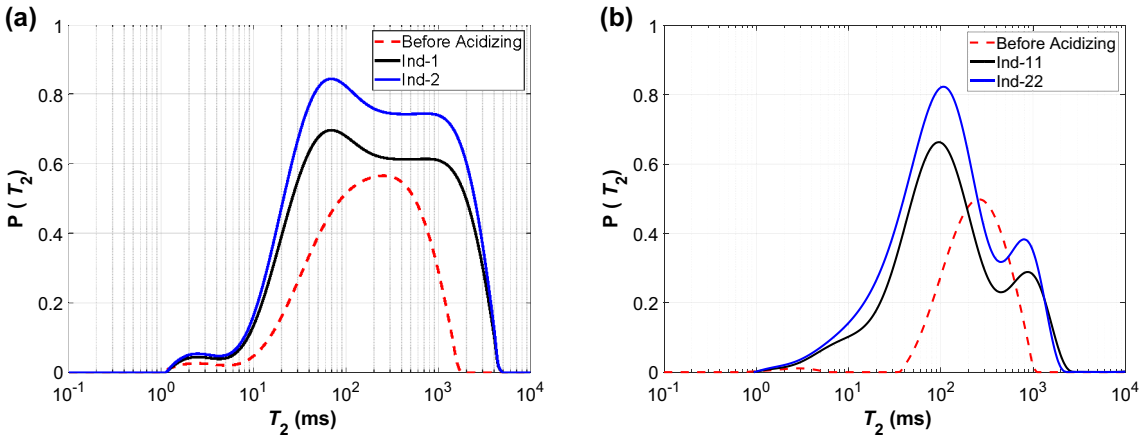

Fig. 5 **a** CT scan images of wormholed sample in set (A) experiments, **b** CT scan images of wormholed sample in set (B) experiments

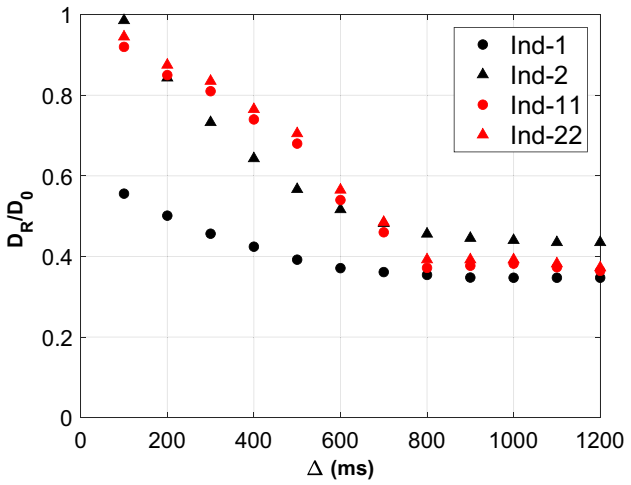

Fig. 6 T_2 relaxation time distributions for the samples studies pre- and post-acidizing **a** samples Ind-1, and Ind-2 **b** samples Ind-11 and Ind-22

Table 6 Scores of the acid diversion efficiency

Scores	Efficiency
$0 < I_d < 0.33$	Poor
$0.34 < I_d < 0.67$	Medium
$0.68 < I_d < 1$	Excellent

showed a reduction of tortuosity only on the Y-direction (see Table 6). This indicates poor diversion where acid did not react significantly in the direction opposite to the wormhole direction. The acid in these cases did not divert itself but followed the least resistance path. To evaluate the diversion capacity, the diversion index (I_d) is postulated in this study which represents the ratio of diffusion tortuosity as shown below:

Table 7 Diffusion tortuosity values along the x- , and y-direction of the rock core plug along with the diversion efficiency index

Set	Sample ID	Base fluid	$\tau_{d,y}$	$\tau_{d,x}$	I_d
	Ind-1	Before acidizing	4.71	4.66	–
A	Ind-1	15% HCl	2.88	4.33	0.665
	Ind-2	15% HCl + 50 lbm/1000 gal PAM	2.30	2.57	0.895
B	Ind-11	15% HCl	2.74	9.35	0.293
	Ind-22	15% HCl + 30 lbm/1000 gal PAM	2.68	8.38	0.319

$$I_d = \frac{\tau_{d,y}}{\tau_{d,x}} \tag{9}$$

where $\tau_{d,y}$ is the diffusion tortuosity in the wormhole direction (Y-Direction) and $\tau_{d,x}$ is the diffusion tortuosity in the orthogonal direction (X-Direction) where the efficiency of the acid diversion can be evaluated as the following Table 6

We propose that the higher the diversion index, the better the diversion capacity of the acid system, as Table 7 indicates. Notice that the diversion index can be compared only to a sister sample. For instance, in this study, Ind-2 could be compared to Ind-1, and Ind-22 to Ind-11. For example, the diversion index ratio of the first experiment set was 1.35, indicating a 35% increase in diversion, while 1.1 for the second set indicated a 10% increase. This is logical as higher concentrations of PAM were utilized in the first set, which improves the diversion efficiency. It is worth mentioning that the values obtained here match very well with the results from our previous study where the carbonate samples where acidized using HCL only that created straight-line wormhole (Elsayed et al. 2021c). The HCl caused a reduction in the diffusion tortuosity in they Y-direction only.

Conclusions

The study showed that the PFG-NMR diffusion tortuosity measurements could quantify the acid diversion efficiency. Straight HCl acid was used to create straight wormholes in limestone samples, while a diverting acid created zig-zagged wormholes, and here are some conclusions that can be drawn from this study:

- The wormhole shapes were visualized through CT scans of the acidized samples, in addition, the NMR diffusion tortuosity measurements were taken in directions parallel and perpendicular to the wormhole path to investigate the diversion efficiency:
- We introduce a new diversion efficiency index (I_d) based on the NMR diffusion measurements. We found that the ratio of the diffusion tortuosity in the wormhole direction to the orthogonal one can quantify acid diversion efficiency.
- Based on the new diversion index, the diversion efficiency of the 50 lbm/ 1000 gal PAM gelled acid was 35% higher compared to the straight HCl acid. On the contrary, the 30 lbm/ 1000 gal PAM gelled acid gave only 10% improvement in the diversion. The index could screen quantitatively which diverting acid is more efficient.

Acknowledgements The authors would like to thank the Collage of Petroleum Engineering and Geosciences, King Fahd University of Petroleum and Minerals for providing all the facilities and materials for this research.

Funding The research did not receive any funding.

Declarations

Conflict of interest The authors declare that they have no known competing financial interests or personal relationships that could have appeared to influence the work reported in this paper.

References

Adewunmi AA, Solling T, Sultan AS, Saikia T (2022) Emulsified acid systems for oil well stimulation: a review. J Pet Sci Eng 208:109569. https://doi.org/10.1016/j.petrol.2021.109569

Alarji H, Alazman A, Regenauer-Lieb K (2022) The impact of effective tortuosity on carbonate acidizing and the validation of Damköhler and Péclet dimensionless phase space. J Pet Sci Eng 212:110313. https://doi.org/10.1016/j.petrol.2022.110313

Al-Duailej YK, Kwak HT, Caliskan S, Al-Yami IS (2013) Wormhole characterisation using NMR. In: All Days. IPTC, p IPTC-17063-MS

Al-Garadi K, El-Husseiny A, Elsayed M et al (2022) A rock core wettability index using NMR T measurements. J Pet Sci Eng 208:109386. https://doi.org/10.1016/j.petrol.2021.109386

Al-Ghamdi AHH, Mahmoud MAA, Wang G et al (2014) Acid diversion by use of viscoelastic surfactants: the effects of flow rate and initial permeability contrast. SPE J 19:1203–1216. https://doi.org/10.2118/142564-PA

Aljawad MS (2020) Impact of diversion on acid fracturing of laminated carbonate formations: a modeling perspective. ACS Omega 5:6153–6162. https://doi.org/10.1021/acsomega.0c00178

Altunina LK, Kuvshinov VA, Stasyeva LA, Kuvshinov IV (2019) Enhanced oil recovery from high-viscosity oil deposits by acid systems based on surfactants, coordining solvents and complex compounds. Georesursy 21:103–113. https://doi.org/10.18599/grs.2019.4.103-113

Ba Alawi M, Hassan A, Aljawad MS et al (2020) A Novel approach to improve acid diversion in carbonate rocks using thermochemical fluids: experimental and numerical study. Molecules 25:2976. https://doi.org/10.3390/molecules25132976

Backeberg NR, Iacoviello F, Rittner M et al (2017) Quantifying the anisotropy and tortuosity of permeable pathways in clay-rich mudstones using models based on X-ray tomography. Sci Rep 7:1–12. https://doi.org/10.1038/s41598-017-14810-1

Blackwell RJ (1962) Laboratory studies of microscopic dispersion phenomena. Soc Pet Eng J 2:1–8. https://doi.org/10.2118/1483-G

Callaghan PT, Coy A, MacGowan D et al (1991) Diffraction-like effects in NMR diffusion studies of fluids in porous solids. Nature 351:467–469. https://doi.org/10.1038/351467a0

Cao C, Zhou F, Cheng L et al (2021) A comprehensive method for acid diversion performance evaluation in strongly heterogeneous carbonate reservoirs stimulation using CT. J Pet Sci Eng 203:108614. https://doi.org/10.1016/j.petrol.2021.108614

Carr HY, Purcell EM (1954) Effects of diffusion on free precession in nuclear magnetic resonance experiments. Phys Rev 94:630–638. https://doi.org/10.1103/PhysRev.94.630

Cheng L, Kam SI, Delshad M, Rossen WR (2002) Simulation of dynamic foam-acid diversion processes. SPE J 7:316–324. https://doi.org/10.2118/79639-PA

Connolly PRJ, Yan W, Zhang D et al (2019) Simulation and experimental measurements of internal magnetic field gradients and NMR transverse relaxation times (T2) in sandstone rocks. J Pet Sci Eng 175:985–997. https://doi.org/10.1016/j.petrol.2019.01.036

Cotts R, Hoch MJ, Sun T, Markert J (1989) Pulsed field gradient stimulated echo methods for improved NMR diffusion measurements in heterogeneous systems. J Magn Reson 83:252–266. https://doi.org/10.1016/0022-2364(89)90189-3

Derendyaev RA, Novikov VA, Martyushev DA et al (2022) Acid treatment of carbonate reservoir with a new dual action microemulsion: Selection of optimal application conditions. J Pet Sci Eng 216:110809. https://doi.org/10.1016/j.petrol.2022.110809

Du J, He Y, Liu P et al (2019) Experimental study of acidizing diversion effect on different permeability of heterogeneity sandstone

reservoirs. J Pet Explor Prod Technol 9:2709–2716. https://doi.org/10.1007/s13202-019-0642-9
Dvir T, Timko BP, Kohane DS, Langer R (2011) Nanotechnological strategies for engineering complex tissues. Nat Nanotechnol 6:13–22. https://doi.org/10.1038/nnano.2010.246
Elsayed M, El-Husseiny A, Kadafur I et al (2021b) An experimental study on the effect of magnetic field strength and internal gradient on NMR-Derived petrophysical properties of sandstones. J Pet Sci Eng 205:108811. https://doi.org/10.1016/j.petrol.2021.108811
Elsayed M, El-Husseiny A, Kwak H et al (2021c) New technique for evaluating fracture geometry and preferential orientation using pulsed field gradient nuclear magnetic resonance. SPE J. https://doi.org/10.2118/205505-PA
Elsayed M, Isah A, Hiba M et al (2022) A review on the applications of nuclear magnetic resonance (NMR) in the oil and gas industry: laboratory and field-scale measurements. J Pet Explor Prod Technol. https://doi.org/10.1007/s13202-022-01476-3
Elsayed M, Ammar E-H, Mahmoud M, Karem A-G (2021a) Method for evaluation of permeability anisotropy using NMR diffusion measurements for oil and gas wells. J Pet Explor Prod Technol 12:2747–2784
Fredd CN, Fogler HS (1998) Influence of transport and reaction on wormhole formation in porous media. AIChE J 44:1933–1949. https://doi.org/10.1002/aic.690440902
Fredd CN, Fogler HS (1999) Optimum conditions for wormhole formation in carbonate porous media: influence of transport and reaction. SPE J 4:196–205. https://doi.org/10.2118/56995-PA
Frosch GP, Tillich JE, Haselmeier R et al (2000) Probing the pore space of geothermal reservoir sandstones by nuclear magnetic resonance. Geothermics 29:671–687. https://doi.org/10.1016/S0375-6505(00)00031-6
Hoefner ML, Fogler HS (1989) Fluid-velocity and reaction-rate effects during carbonate acidizing: application of network model. SPE Prod Eng 4:56–62. https://doi.org/10.2118/15573-PA
Hurlimann MD, Helmer KG, Latour LL, Sotak CH (1994) Restricted diffusion in sedimentary rocks. determination of surface-area-to-volume ratio and surface relaxivity. J Magn Reson Ser A 111:169–178. https://doi.org/10.1006/jmra.1994.1243
Kashif M, Cao Y, Yuan G et al (2019) Pore size distribution, their geometry and connectivity in deeply buried Paleogene Es1 sandstone reservoir, Nanpu Sag, East China. Pet Sci 16:981–1000. https://doi.org/10.1007/s12182-019-00375-3
Kenyon WE (1997) Petrophysical principles of applications of NMR logging. Log Anal 38:23
Kolitcheff S, Jolimaitre E, Hugon A et al (2018) Tortuosity and mass transfer limitations in industrial hydrotreating catalysts: effect of particle shape and size distribution. Catal Sci Technol 8:4537–4549. https://doi.org/10.1039/C8CY00831K
Latour LL, Mitra PP, Kleinberg RL, Sotak CH (1993) Time-dependent diffusion coefficient of fluids in porous media as a probe of surface-to-volume ratio. J Magn Reson Ser A 101:342–346. https://doi.org/10.1006/jmra.1993.1056
Liu J, Liu X-W (2012) Two-dimensional nanoarchitectures for lithium storage. Adv Mater 24:4097–4111. https://doi.org/10.1002/adma.201104993
Liu N, Liu M (2016) Simulation and analysis of wormhole propagation by VES acid in carbonate acidizing. J Pet Sci Eng 138:57–65. https://doi.org/10.1016/j.petrol.2015.12.011
Long JW, Dunn B, Rolison DR, White HS (2004) Three-dimensional battery architectures. Chem Rev 104:4463–4492. https://doi.org/10.1021/cr020740l
Mahmoud M, Al-Duailej Y, Al-Khaldi M et al (2016) NMR as a characterization tool for wormholes. SPE Prod Oper 31:362–373. https://doi.org/10.2118/171699-PA
Martyushev DA, Vinogradov J (2021) Development and application of a double action acidic emulsion for improved oil well performance: laboratory tests and field trials. Colloids Surfaces A Physicochem Eng Asp 612:125998. https://doi.org/10.1016/j.colsurfa.2020.125998
Martyushev DA, Govindarajan SK, Li Y, Yang Y (2022) Experimental study of the influence of the content of calcite and dolomite in the rock on the efficiency of acid treatment. J Pet Sci Eng 208:109770. https://doi.org/10.1016/j.petrol.2021.109770
Martyushev D, Novikov V (2020) Improving acidizing in the collectors characterized by different carbonate content (on the example of oil fields of Perm Krai). Geo Assets Eng. https://doi.org/10.18799/24131830/2020/9/2800
Meiboom S, Gill D (1958) Modified spin-echo method for measuring nuclear relaxation times. Rev Sci Instrum 29:688–691. https://doi.org/10.1063/1.1716296
Novikov VA, Martyushev DA, Li Y, Yang Y (2022) A new approach for the demonstration of acidizing parameters of carbonates: experimental and field studies. J Pet Sci Eng 213:110363. https://doi.org/10.1016/j.petrol.2022.110363
Panga MKR, Ziauddin M, Balakotaiah V (2005) Two-scale continuum model for simulation of wormholes in carbonate acidization. AIChE J 51:3231–3248. https://doi.org/10.1002/aic.10574
Sen PN (2004) Time-dependent diffusion coefficient as a probe of geometry. Concepts Magn Reson Part A Bridg Educ Res 23:1–21. https://doi.org/10.1002/cmr.a.20017
Shafiq MU, Ben Mahmud HK, Arif M (2018) Mineralogy and pore topology analysis during matrix acidizing of tight sandstone and dolomite formations using chelating agents. J Pet Sci Eng 167:869–876. https://doi.org/10.1016/j.petrol.2018.02.057
Stejskal EO, Tanner JE (1965) Spin diffusion measurements: spin echoes in the presence of a time-dependent field gradient. J Chem Phys 42:288–292. https://doi.org/10.1063/1.1695690
Straley C, Roosini D, Vinegar HJ et al (1997) Core analysis by low-field NMR. Log Anal 38:84–94
Strongylis P, Papamichos E (2021) Analytical solutions of carbonate acidizing in radial flow. Transp Porous Media 139:223–245. https://doi.org/10.1007/s11242-021-01657-4
Timur A (1969) Pulsed nuclear magnetic resonance studies of porosity, movable fluid, and permeability of sandstones. J Pet Technol 21:775–786. https://doi.org/10.2118/2045-PA
Vogt SJ, Shaw CA, Maneval JE et al (2014) Magnetic resonance measurements of flow-path enhancement during supercritical CO2 injection in sandstone and carbonate rock cores. J Pet Sci Eng 122:507–514. https://doi.org/10.1016/j.petrol.2014.08.013
Wu Y, Kou J, Sun S (2022) Matrix acidization in fractured porous media with the continuum fracture model and thermal Darcy-Brinkman-Forchheimer framework. J Pet Sci Eng 211:110210. https://doi.org/10.1016/j.petrol.2022.110210
Yang K, Li M, Ling NNA et al (2019) Quantitative tortuosity measurements of carbonate rocks using pulsed field gradient NMR. Transp Porous Media 130:847–865. https://doi.org/10.1007/s11242-019-01341-8
Yoo H, Park J, Lee Y, Lee J (2019) An experimental investigation into the effect of pore size distribution on the acid-rock reaction in carbonate acidizing. J Pet Sci Eng 180:504–517. https://doi.org/10.1016/j.petrol.2019.05.061
Zakaria AS, Nasr-El-Din HA (2016) A Novel polymer-assisted emulsified-acid system improves the efficiency of carbonate matrix acidizing. SPE J 21:1061–1074. https://doi.org/10.2118/173711-PA
Zerhboub M, Ben-Naceur K, Touboul E, Thomas R (1994) Matrix acidizing: a novel approach to foam diversion. SPE Prod Facil 9:121–126. https://doi.org/10.2118/22854-PA
Zhang L, He J, Wang H et al (2021) Experimental investigation on wormhole propagation during foamed-VES acidizing. J Pet Sci Eng 198:108139. https://doi.org/10.1016/j.petrol.2020.108139